Journal of Applied Fluid Mechanics, Vol. 16, No. 12, pp. 2494-2503, 2023.
Available online at www.jafmonline.net, ISSN 1735-3572, EISSN 1735-3645.
https://doi.org/10.47176/jafm.16.12.1865

Supersonic Flow over Elliptic Cone with Different Ellipticity Ratio

V. Kotebavi† and S. G. Rakesh

Department of Mechanical Engineering, Amrita School of Engineering, Bengaluru, Amrita Vishwa Vidyapeetham, India

†*Corresponding Author Email: k_vinod@blr.amrita.edu*

ABSTRACT

This study investigates supersonic flow characteristics over circular and elliptic cones at various angles of attack. Simulations were conducted on the cones with the same base area and length-to-diameter ratio. The elliptic cones considered had axis ratios of 1.5 and 3. The angle of attack varied from 0º to 50º, with two different Mach numbers (1.97 and 2.94) employed for the analysis. The numerical results were compared with the experimental and theoretical findings from existing literature. The results revealed that increasing the ellipticity ratio of the cones resulted in higher lift generation. The pressure distributions on the windward and leeward sides of the cones were also examined. The results demonstrated that elliptic cones outperformed circular cones in terms of lift production, and this advantage increased with higher ellipticity ratios. Specifically, when the ellipticity ratio was increased from 1 to 3, the maximum increase in lift coefficient was 96% and 100% at Mach numbers 2.94 and 1.97, respectively. Additionally, by changing the ellipticity ratio from 1 to 1.5, the maximum gain in the lift-drag ratio was 16% and 22% at Mach numbers 1.97 and 2.94, respectively. Notably, an elliptic cone with an ellipticity ratio of 3 achieved a remarkable 46% gain in lift-to-drag ratio compared to a circular cone. However, as the angle of attack increased, a primary bow shock formed on the windward side of the cone, with an embedded shock appearing on the leeward side.

Article History

Received March 7, 2023
Revised July 28, 2023
Accepted July 31, 2023
Available online October 8, 2023

Keywords:

Elliptic cone
Supersonic flow
Mach number
Lift
Drag

1. INTRODUCTION

The aerodynamic characteristics of vehicles that fly at supersonic speeds are very important. However, many theoretical methods and data are available to obtain aerodynamic characteristics for bodies of revolution. However, the information on noncircular bodies at higher angles of incidence is limited. The circular cone can be considered as standard of comparison for flow past bodies of revolution, whereas the elliptical cone plays the same role for bodies with noncircular cross-sections. Many numerical solutions and data are available for circular cones, but the solutions for elliptic cones are yet to be established, specifically at higher angles of attack. Taylor and Maccoll (1933) obtained solutions by numerical integration for circular cones in supersonic flow at zero angle of attack. This solution was limited to circular cones with semi-vertex angles 10º, 20º, and 30º. They also conducted experiments on these cones in a high-speed wind tunnel. Excellent agreement was found between the theoretically calculated and experimentally obtained pressure values. Ishimatsu and Morishita (2005) obtained analytical solutions for Taylor and Maccoll equations. These equations are valid only for cones with semi-vertex angles less than 30º. This is because the normal velocity component becomes very small on the surfaces only when the semi-vertex angle is less than 30º. Dyke (1956) derived the second-order slender body solutions for elliptic cones in supersonic flows. Since then, many researchers worked on it to make tables for cones in supersonic flow at zero angle of attack (Kopal, 1947; Sims, 1964). Saiprakash et al. (2019) conducted experiments on the sharp cone at 0º and 5º angles of attack to study the flow field at Mach number 6.5. They captured shock around the cone using the Schlieren technique. The shock layer thickness obtained from the experiments was very close to the results obtained from the computational study.

In high-speed flow, it is very important to reduce the drag experienced by the vehicle as it reduces the thrust required for the propulsion. The drag can be reduced in conical bodies by making the body slender and sharp. However, upon doing so, heat transfer increases. Thus, designing a high-speed vehicle with lower drag and heat transfer is very challenging. Many attempts have been

NOMENCLATURE

A	semi major axis	*Re*	Reynolds number
B	semi minor axis	δ	ellipticity ratio
AOA	Angle of Attack	θc	semi-apex angle of a circular cone
Cd	drag coefficient	θy	semi-vertex angle in a vertical plane
Cl	lift coefficient	θz	semi-vertex angle in a horizontal plane
l/d	fineness ratio		

made to reduce the aerodynamic drag by modifying the geometry. Using spikes (Sreekanth et al., 2016; Krishnan et al., 2017) in blunted cones reduced drag considerably. However, this introduces an undesirable pulsation phenomenon (Rajesh & Rakesh, 2017, 2020) in some geometries. Subsequently, to mitigate such challenges, Krishna & Kotebavi (2021) used blunted power law bodies to reduce drag and heat transfer.

While high-speed flow research has predominantly focused on bodies with circular cross-sections, noncircular cross-sections have garnered significant interest among researchers. Chen et al. (2020) performed an optimization study on different noncircular fore body shapes. They tried to optimize the cross-section for better aerodynamic efficiency. Some experimental and numerical works have been done on noncircular cross sections like square, elliptic, and diamond shapes. Elliptic cones are considered efficient compared to circular cones for better lift and drag characteristics over a wide range of speeds (Jorgensen, 1957). Elliptic cones are mainly specified by the ellipticity ratio, defined as the ratio of the major axis (A) to the minor axis (B) and fineness ratio, i.e., the length-to-base diameter. The relation (Kaattari, 1970) between semi apex angle of the circular cone (θ_c) and the semi-vertex angles of an equivalent elliptic cone is given by Eq. (1).

$$Tan\,\theta_c = \sqrt{[(Tan\,\theta_y)(Tan\theta_z)]} \quad (1)$$

Where θ_y and θ_z are the semi-vertex angles in the plane of the minor and major axis, respectively. This equation helps to calculate the elliptic cone's base dimensions for a given δ and l/d ratio.

Jorgensen (1957) conducted experiments on elliptic cones in supersonic wind tunnel at Mach numbers 1.97 and 2.94. In his experiments, he used elliptic cones with ellipticity ratios of 1.5, 3, and 6 and varied angles of attack from 0° to 14°. Experiments were also conducted with wings on elliptic cones. The aerodynamic advantages of elliptic cones over circular cones were reported in the results. When the triangular wings were attached to the elliptic cone, they produced an even higher lift than the circular cone with wings. The experimental results were verified with Dyke's (1956) slender body theory.

Bashkin et al. (2008) investigated the performance and flow structure around the elliptic cone in supersonic flow over a wide range of ellipticity ratios. The transverse flow was not observed at zero angles of attack, but it begins as the angle of attack increases. The flow regime also changes as the ellipticity ratio changes. It was also observed that the pressure drag and the heat flux reduces as the ellipticity ratio increases. Bashkin et al. (2009) performed numerical investigations on elliptic cones to study the aerodynamic characteristics. They observed higher pressure on major axis and lower pressure on minor axis. Kahane & Solarski (1953) described a theory to obtain pressure distribution on cones with elliptic cross sections. It was found that the wave drag in the case of the elliptic cone is lower when compared to the circular cone of the same base area. Using the perturbation method, Rahimi (2012) studied the aerodynamic characteristics of cones with different cross sections like circular, elliptic, and squircle. It was concluded that the lift drag ratio is maximum for squircle and minimum for circular cone. Pedro et al. (2013) derived Parabolic, steady, 3-dimensional Navier-Stokes equations to study the flow over circular and elliptic cones in supersonic flow. They obtained boundary layer solutions at zero angles of attack for circular cones and compared them with theoretical solutions. Nithin and Kotebavi (2022) studied the elliptic cone's pressure distribution and lift drag characteristics in high-speed flow with different ellipticity ratios. The study reported leeward side flow separation at a higher angle of attack.

The literature review reveals a notable research gap in investigating elliptic cones under supersonic flow conditions, particularly at higher angles of attack and with a limited study on shock shapes. Previous studies have primarily focused on slender elliptic cones, leaving room for further exploration in these areas. The present work aims to study the aerodynamic performance, pressure distribution, shock shape, and flow structure of an elliptic cone in supersonic flow at higher angles of attack. Elliptic cones with ellipticity ratios of 1.5 and 3 have been considered for the study. A circular cone with the same base area has also been included in the study for comparison.

The significance of this research lies in its potential to advance our understanding of the fundamental physics of supersonic flow and provide critical information for the design and optimization of high-speed aerospace. By analyzing pressure distributions, shock shapes, and lift and drag coefficients on an elliptic cone, researchers can develop more precise predictive models for understanding the behavior of supersonic vehicles. This, in turn, enables the creation of more efficient and reliable designs with improved performance characteristics.

2. MODEL AND SIMULATION

The study considered two sharp elliptic cones with different ellipticity ratios and a circular cone of the same base area. The base diameter of the circular cone was 5.59 cm. The ratio of major to minor diameters of the elliptic cones was 1.5 and 3. The l/d ratio (length-to-

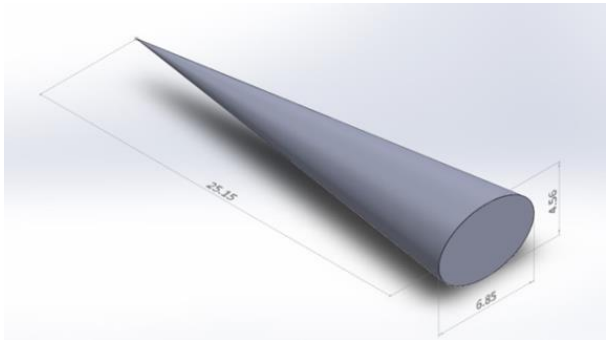

Fig. 1 Dimensions of Elliptic cone with ellipticity ratio 1.5

equivalent diameter of the base) for the cones was 4.5. The 3-D model of the elliptic cone (Major diameter = 6.85 cm, Minor diameter = 4.56 cm) with an ellipticity ratio of 1.5 is shown in Fig. 1.

ANSYS Fluent was used to perform simulations. Simulations were conducted at Mach numbers 1.97 and 2.94 with unit Reynolds numbers (Re/l) of 4.4×10^7 and 6.6×10^7, respectively. The angle of attack varied from 0^o to 45^o. Based on the literature survey we have tried out standard K-ω model and compared with Spalart-Allmaras (S-A) model. We noticed that the variance of results between the two models were 1.5% (Cd) and 2% (Cl). The convergence of results was faster in S- A than K-ω model, so we chose S-A model for all our simulations. The S-A one-equation turbulence model was used with the standard values of model constants. This model solves simple transport equations for the kinematic eddy viscosity and is mainly used for aerospace applications involving wall-bounded flows. The governing equations used are shown below.

1. Continuity equation

$$\frac{\partial \rho}{\partial t}+\frac{\partial(\rho u_i)}{\partial x_i}=0 \tag{2}$$

2. Momentum equation

$$\frac{\partial(\rho u_i)}{\partial t}+\frac{\partial(\rho u_i \rho u_j)}{\partial x_j}=-\frac{\partial p}{\partial x_i}+\frac{\partial \tau_{ij}}{\partial x_j} \tag{3}$$

3. Energy equation

$$\frac{\partial(\rho E)}{\partial t}+\frac{\partial(H u_j)}{\partial x_j}=\frac{\partial p}{\partial x_j}(u_i \tau_{ij}-q_j) \tag{4}$$

4. Spalart-Allamaras transport model equation

$$\frac{\partial}{\partial t}(\rho \nu)+\frac{\partial}{\partial x_i}(\rho \nu u_i) = T_\nu+\frac{1}{\sigma_\nu}\{\frac{\partial}{\partial x_i}\left[(\mu+\rho\nu)\frac{\partial \nu}{\partial x_j}\right] + C_b\,\rho\left(\frac{\partial \nu}{\partial x_j}\right)^2\}-D_\nu+S\nu \tag{5}$$

Where q_j is the heat flux, H total enthalpy, T_ν turbulent viscosity generation, D_ν eddy viscosity destruction, S user-defined source term, C_b and σ_ν are the constants, and ν the molecular kinematic viscosity. The above equations are used for unsteady flow, but steady-state analysis has been carried out in this work. Pressure far-field boundary conditions were used at all boundaries, i.e., inlet, outlet, and side wall, while no-slip with constant temperature boundary condition was used at the body wall. Simulations were carried out for different mesh sizes to study the effect of mesh size on the results. In the case of the elliptic cone with an ellipticity ratio of 1.5, meshes were generated with 1.25 million, 1.6 million, and 2.05 million elements. The results obtained with 1.6 million and 2.05 million were very close. Hence, simulations with 1.6 million elements were carried out to reduce the computational cost.

3. RESULTS AND DISCUSSIONS

Simulations were conducted for two elliptic cones with different ellipticity ratios and a circular cone of the same base area. Different characteristics like drag and lift coefficients were used to compare the performance of these cones at Mach numbers of 1.97 and 2.94.

Figure 2 shows the variation of Cd with the angle of attack for Mach numbers 2.94 and 1.97, respectively.

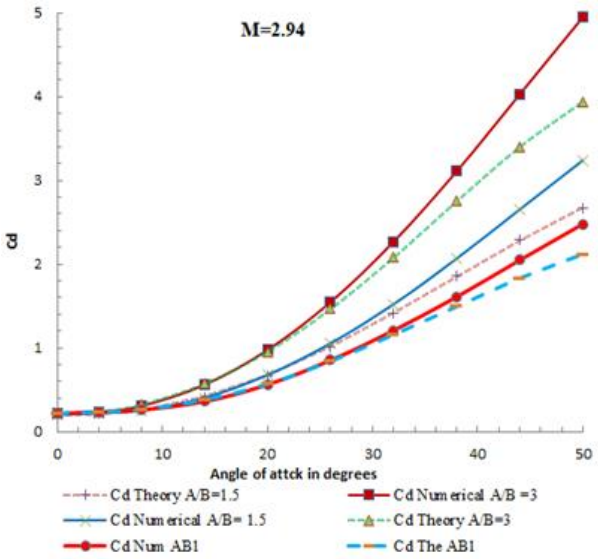

(a) M=2.94

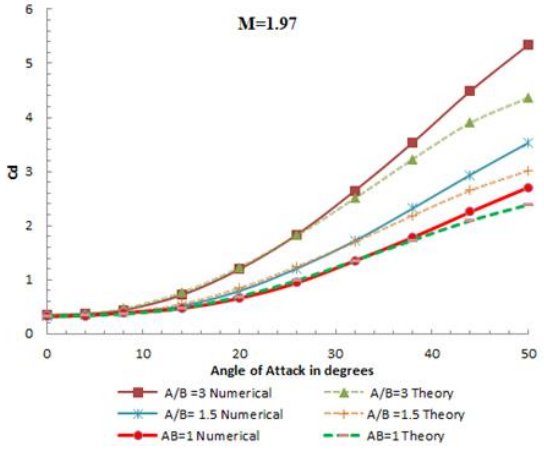

(b) M=1.97

Fig. 2 Comparison of theoretically & numerically obtained C_d values

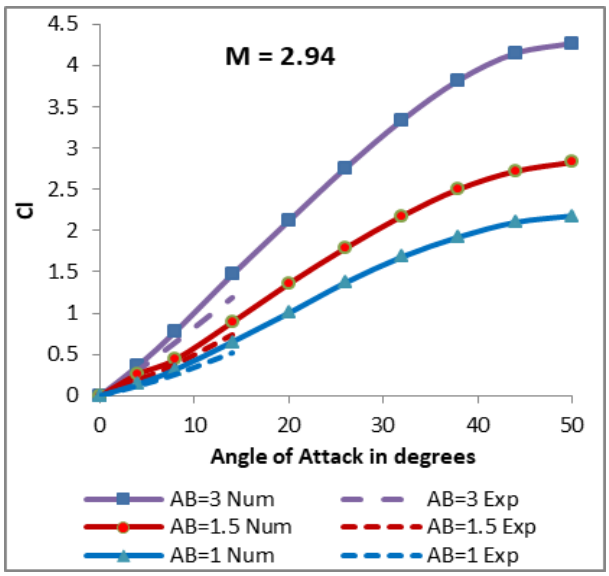

(a) M=2.94

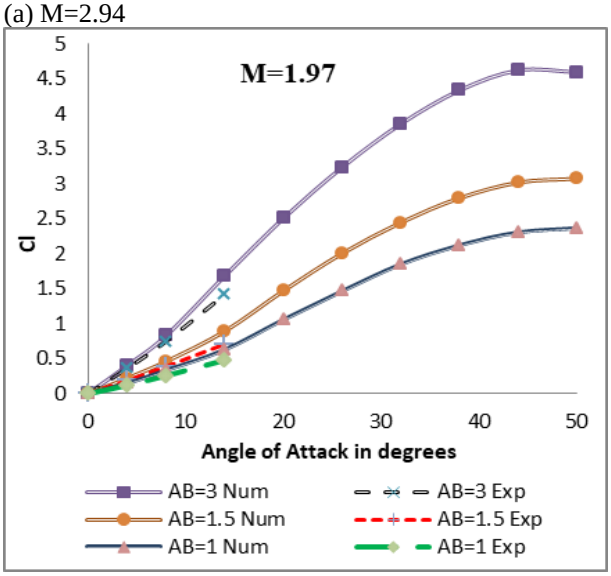

(b) M=1.97

Fig. 3 Effect of ellipticity ratio on the coefficient of lift at different angles of attack

Numerically obtained Cd values are compared with those obtained from theory (Allen et al., 1951). Both results were very close at a lower angle of attack, but the numerical values were a little over-predicted at a higher angle of attack. It was also observed that drag exhibits a slower increase at lower angles of attack. However, as the angle of attack escalates, the rate of drag increase becomes more pronounced.

Figure 3 depicts the variations of lift coefficients with ellipticity ratio at various angles of attack. All the cones used here were of the same base area and length. Jorgensen (1957) conducted experiments with similar conditions up to the angle of attack 14°. His results are also plotted in the same figure, and the numerical results are in close agreement with the experimental results. It can be observed that as the ellipticity ratio increases, the lift coefficient increases. Figures 2 and 3 clearly show that as the ellipticity ratio increases, the drag coefficient and lift coefficient increases, but the lift coefficient increases faster than the drag coefficient. For example, at Mach number 1.97 for an angle of attack 14°, when the ellipticity ratio is increased from 1.5 to 3, the lift increases by 88%, whereas the drag increases only by 40%. It is crucial to know the effect of the ellipticity ratio on the aerodynamic efficiency, can be determined by lift-drag ratio. Figure 4 shows a significant gain in lift-drag ratio throughout the range of investigated angles when the ellipticity ratio is varied from 1 to 3. By changing the ellipticity ratio from 1 to 1.5, the maximum gain in lift-drag ratio results in 16% and 22% for Mach numbers 1.97 and 2.94, respectively.

Furthermore, increasing the ellipticity ratio to 3 from 1 result in a gain of the maximum lift-drag ratio of about 46% at both Mach numbers considered. The aerodynamic efficiency can be improved for a body of a given volume by deviating from a circular to an elliptic cross-section. The increase in lift with ellipticity ratio is due to the increase in pressure on the windward side with an increase in ellipticity ratio, which is discussed in the later sections. The maximum lift-drag ratio for a given cross-section also depends on the Mach number. The increase in Mach number increased the lift-drag ratio for both the elliptic cones. For an ellipticity ratio of 3, the maximum lift-drag ratio increased by 11% when the Mach number increased from 1.97 to 2.94. It is also observed that the angle of attack at which the peak lift-drag ratio occurred decreases with an increase in the ellipticity ratio.

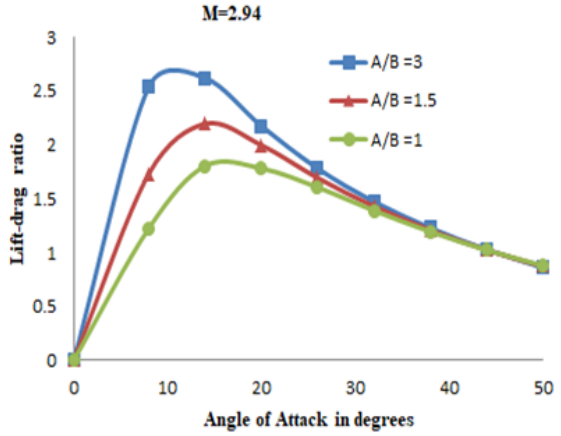

(a) M=2.94

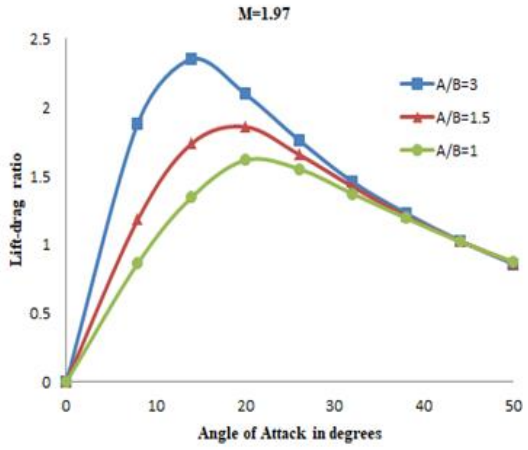

(b) M=1.97

Fig. 4 Lift-drag ratio vs. Angle of attack

Table 1 Friction drag, and pressure drag coefficients at M=2.94

Ellipticity ratio	Pressure drag Coefficient	Friction Drag Coefficient
1	0.194	0.018
1.5	0.188	0.0227
3	0.1857	0.028

The drag coefficients at zero angle of attack for different ellipticity ratios are found to be constant but vary with the Mach number. At Mach number 1.97, it is 0.33, whereas, for Mach number 2.94, it is 0.21. The zero-lift drag remains constant for the same volume and fineness ratio at a given Mach number. Similar results were obtained by Jorgensen (1957) during his experiments. Taylor and Maccoll's (1933) circular cone theory also predicts the same drag coefficient for a circular cone at zero angles of attack. The skin friction drag increases with the ellipticity ratio because of the higher wetted surface area. This increase in drag is enough to nullify the pressure drag saved because of the higher ellipticity ratio. Friction and pressure drag coefficients for different cones at M=2.94 are tabulated (Table 1).

Taylor-Maccoll's (1933) equation is derived for supersonic flow over a circular cone at zero angle of attack. This equation helps to find the shock cone angle for conical shock. Shock formation occurs when a body is placed in a fluid moving at a velocity greater than Mach number 1. Inside the shock is a sudden rise in density, temperature, and pressure (Wang & Kong, 2023). The density contour for a circular cone at M=2.94 for zero angles of attack is shown in Fig.5. The semi-cone angle for the selected cone is 6.34º. The shockwave angle from the simulation is 21º whereas the shockwave angle obtained from the conical shock table is 20.43º and from the analytical solution (Ishimatsu & Morishita, 2005) is 20.67º. The corresponding values for the Mach number 1.97 are 31º, 30.74º, and 31.4º, respectively. The shockwave angles obtained from all the above three methods are in close agreement.

The pressures inside the shock at different angles are measured and compared with the theoretical results. The pressure ratio (static pressure to the stagnation pressure after the shock) obtained from the simulation is compared with that obtained by Taylor and Maccol solution (1933) in Fig. 6. Numerically obtained results are very close to the theoretical solutions.

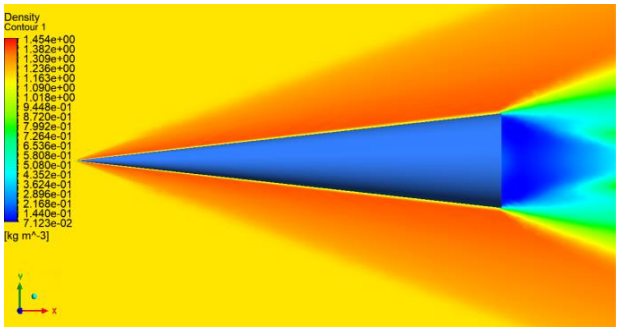

Fig. 5 Density contour for a circular cone at M=2.94

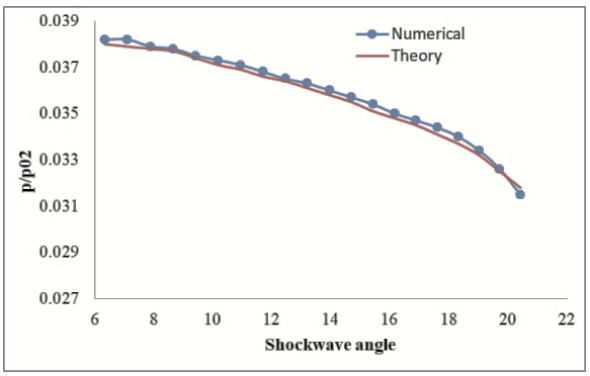

Fig. 6 Pressure ratio inside the shock wave vs. shockwave angle

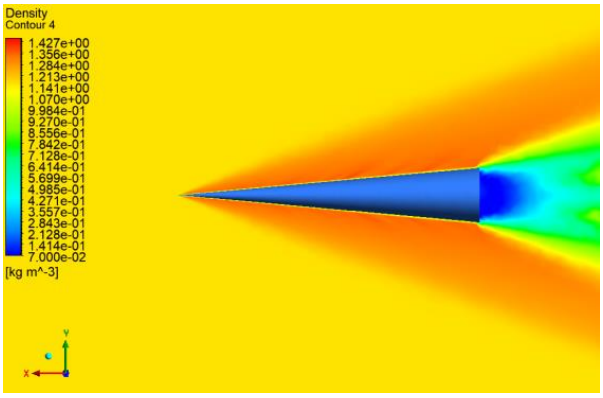

(a) Minor axis plane

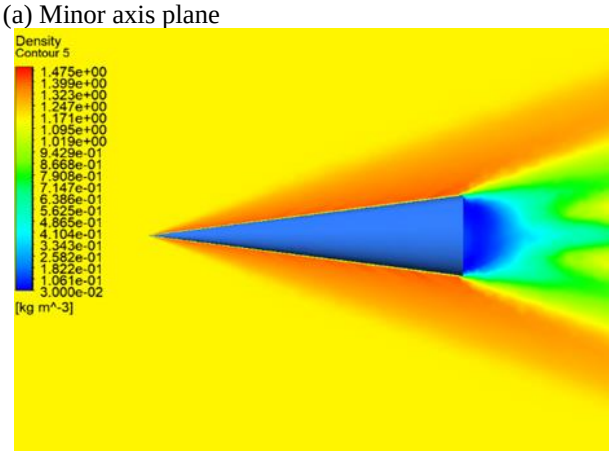

(b) Major axis plane

Fig. 7 Density contour for Elliptic cone with A/B =1.5 at M=2.94

Since the flow of a circular cone is axisymmetric, the streamlines remain in the meridian plane. No cross-flow is observed here. In the case of an elliptic cone, the flow becomes three-dimensional, producing pressure gradients in the lateral directions, which induces cross-flow. Because of this, in elliptic cone flow, two main regions are observed, on the leading edge an attachment line (major axis) and the top center line (min or axis), where the lift up is seen.

The density contours for an elliptic cone with an ellipticity ratio of 1.5 for M=2.94 is shown in Fig.7. Figure 7 a. is in the minor axis (vertical) plane & b. is in the major axis (horizontal) plane. It can be seen that even though the semi-cone angles in the minor and major axes are different, the shock wave angles appear to be the

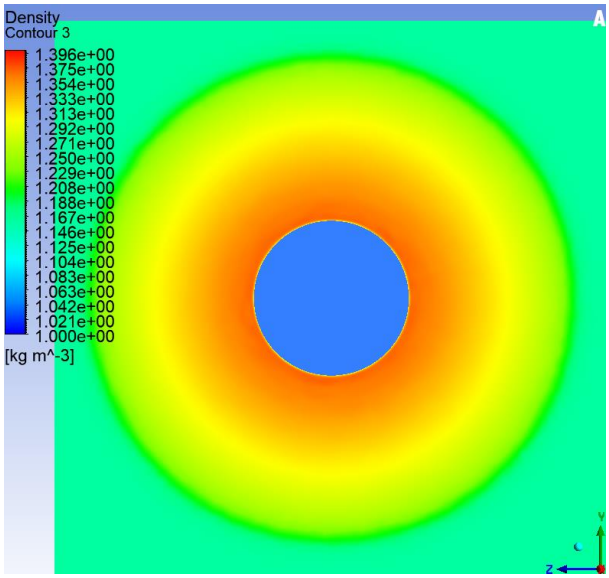

(a) Circular Cone

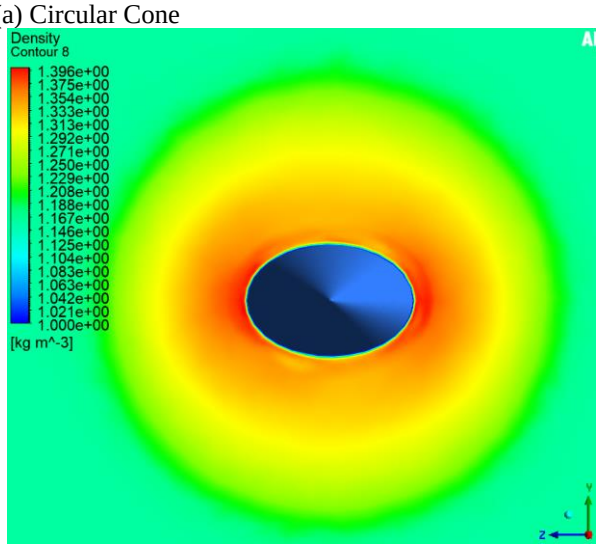

(b) Elliptic cone with A/B = 1.5

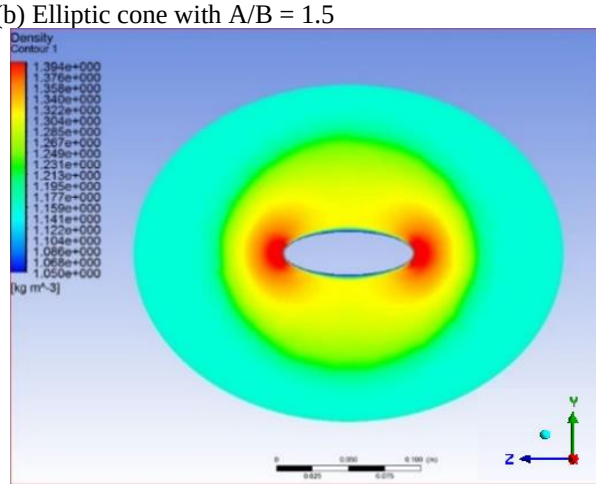

(c) Elliptic cone with A/B = 3

Fig. 8 Shock shape in a plane perpendicular to the axis at zero angles of attack

same in both planes. When the angle of attack exceeds the cones semi-vertex angle (in the plane of the minor axis), the leeside flow separation (axial direction) starts in the vertical plane. Figure 8 presents the shock shapes captured in planes (y-z planes) perpendicular to the axis of both the circular and elliptic cones. Notably, the shock shape in the circular cone appears circular, and similarly,

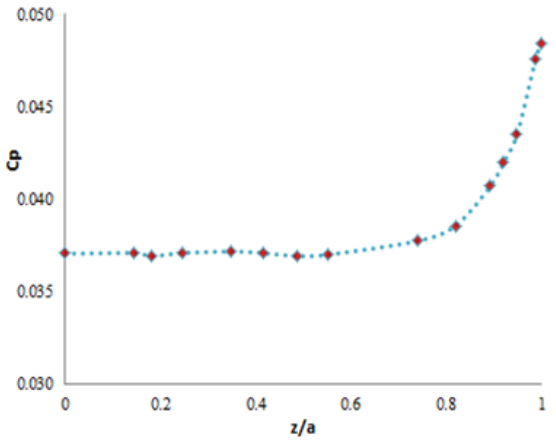

Fig. 9 Pressure distribution on the cone surface

the shock shape seems to be circular in the case of the elliptic cone as well. A distinct observation is that the shock thickness is smaller along the major axis plane than the minor axis plane. Similar observations were made by Bashkin et al. (2009). This suggests that the shock is compressed inward along the major axis plane and pushed outward along the minor axis plane. This is because the cross-flow from the leading edges to the center line and the pressure around the leading is more than the center line. This is evident from the pressure distribution curve in Fig 9.

Pressure distribution on the elliptic cone surface for M=2.94 at zero angles of attack is shown in Fig. 9. The pressure coefficient is plotted against the lateral distance, z/a, over a quadrant of an elliptic cone with an ellipticity ratio of 1.5. Here z is the distance measured along the major axis from the cone's axis, and a is the semi-major axis. Pressure values are measured on a plane at a distance of 0.12 m from the base. A similar trend was seen in Jorgensen's (1957) experiments. This plot shows that maximum pressure occurs at the leading edge, i.e., at the major axis, and minimum at the minor axis. This pressure plot is symmetric about the minor axis.

The normalized pressure on the surface of the elliptic cone with an ellipticity ratio of 1.5 for different angles of attack (0^o, 20^o, and 45^o) at M=2.94 is shown in Fig. 10. The abscissa represents the angle measured from the major axis, which is positive on the leeward side and negative on the windward side. The normalized pressure profile for zero angles of attack is relatively flat, with a small rise at the leading edge. This trend is broken at a higher angle of attack. Very high pressures are observed on the windward side compared to the leading edge. Windward side pressure increases with the angle of attack, resulting in higher lift. The difference in windward and leeward side pressure increases with the ellipticity ratio. Due to this, the lift increases with the ellipticity ratio.

Figure 11 shows the density contours for circular and elliptic cones at Mach number 2.94 and the angle of attack 8^o. It shows that the shock is more attached to the windward side's elliptic cone, which also results in higher pressure creating a higher lift in the elliptic cone.

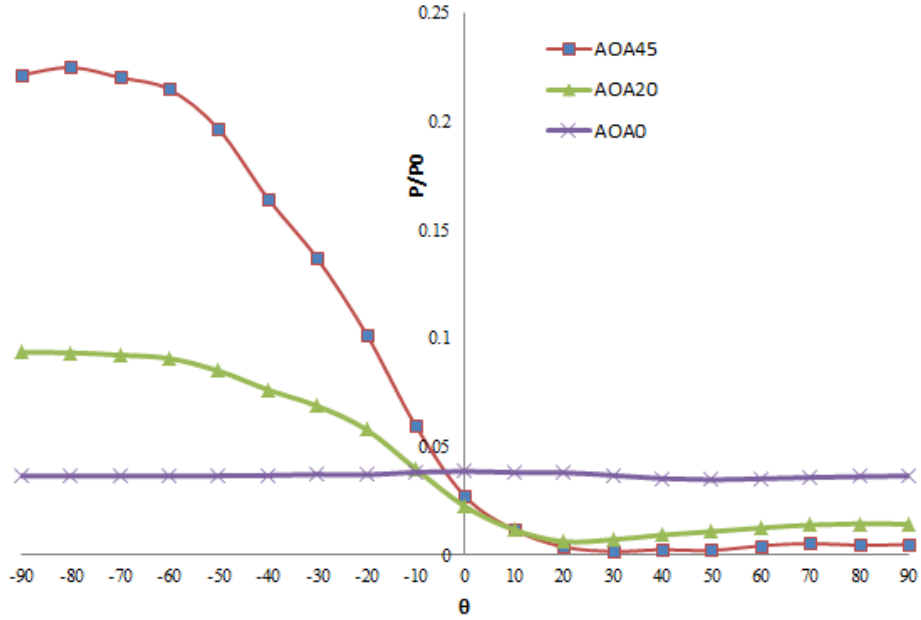

Fig. 10 Normalized pressure distribution

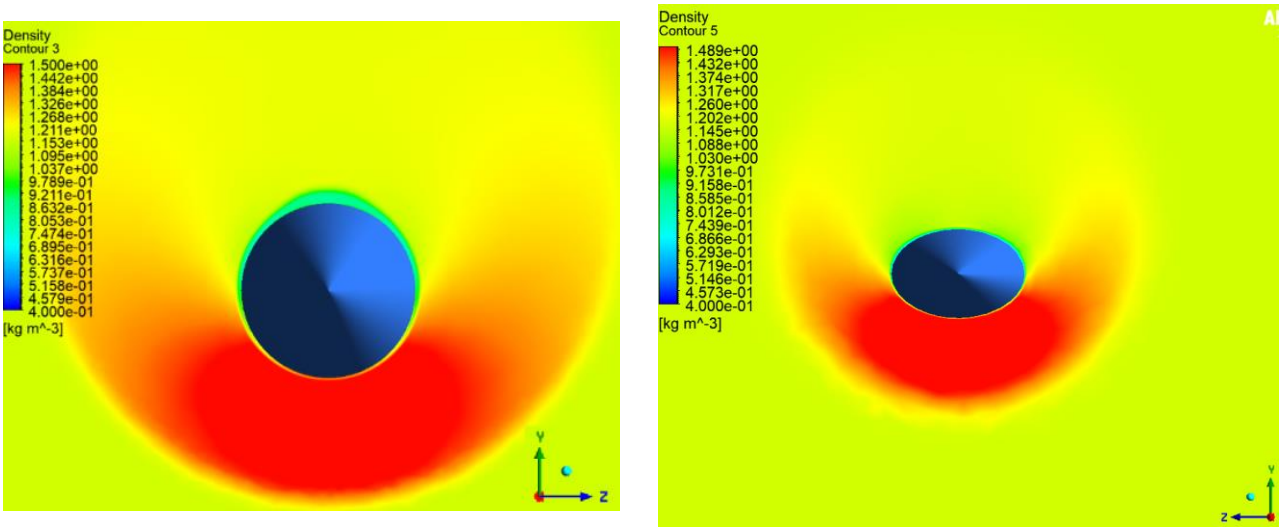

(a) Circular cone (b) Elliptic cone

Fig. 11 Density contour at M= 2.94 & AOA =8º for a) circular cone b) elliptic cone

Figure 12 illustrates the span-wise (z-direction) velocity component for the elliptic cone with an ellipticity ratio of 1.5 at various angles of attack. All the contours in the figure are normalized with a single legend. As the angle of attack increases, there is a notable alteration in the flow pattern on both the windward and leeward sides. Flow expansion and separation are on the leeward side, while a strong shock is present on the windward side. As the flow moves from the windward side to the leeward side (cross flow), it decelerates, initiating leeside flow separation with a pair of symmetrical vortices, gradually forming an embedded shock. This embedded shockwave occurs due to the deceleration of the w-component (cross flow) of velocity, transitioning from supersonic to subsonic velocities, as evident in Fig. 12 to Fig. 14. The magnitude of this velocity component intensifies with increasing angles of attack, thereby augmenting the strength of the shock.

Furthermore, with an increase in the angle of attack, the shock waves become elongated in the upward direction. In the case of circular cones, the embedded shocks remain vertical, whereas elliptic cones bend inward as the ellipticity ratio increases. Similar observations were made for an elliptic cone with an ellipticity ratio of 3 (Fig. 13).

Figure 15 shows the velocity streamlines at different angles of attack for Mach number 2.94. These streamlines are drawn on a plane perpendicular to the axis. No flow separation is observed in this plane till the angle of attack 4º. Flow separation starts when the angle of attack exceeds the semi-vertex angle. For the cone considered, the semi-vertex angle is 5.18º. The magnitude of flow separation increases as the angle of attack increases. Vortices are seen on the leeward side, and this vortex structure gets reattached to the top center line. The line of convergence and divergence were observed from the surface streamlines on the leeward side. They move towards the apex as the angle of attack increases.

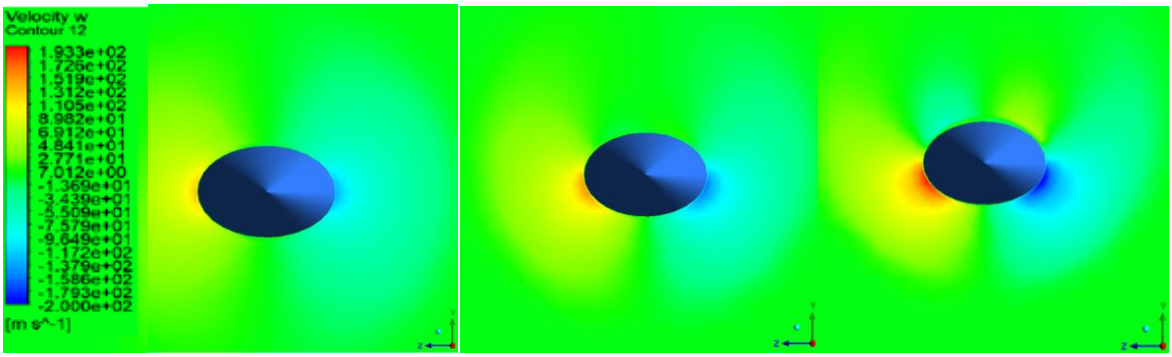

(a) AOA=0º (b) AOA=4º (c) AOA=8º

(d) AOA=20º (e) AOA=30º (f) AOA=45º

Fig. 12 Span-wise Velocity Contour for different AOA for the elliptic cone with A/B=1.5

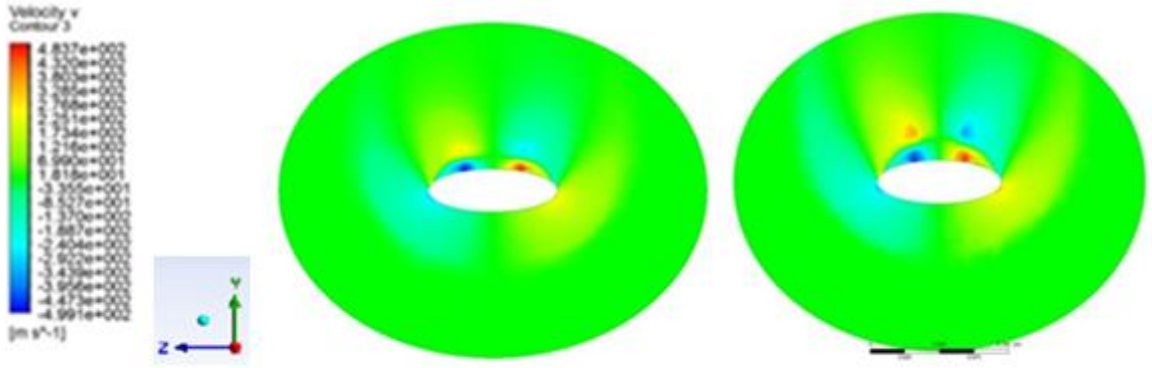

(a) AOA = 14º (b) AOA = 20º

Fig. 13 Span-wise Velocity Contours at AOA 14º & 20º for the elliptic cone with A/B =3

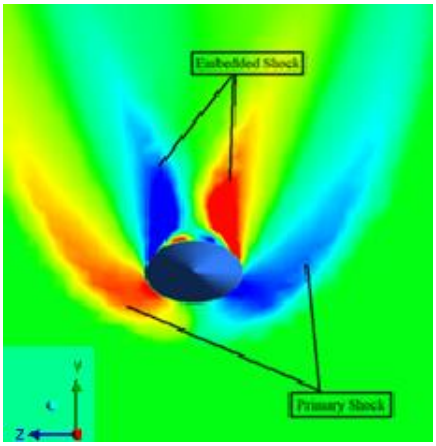

Fig. 14 Primary and Embedded Shock at AOA 45º.

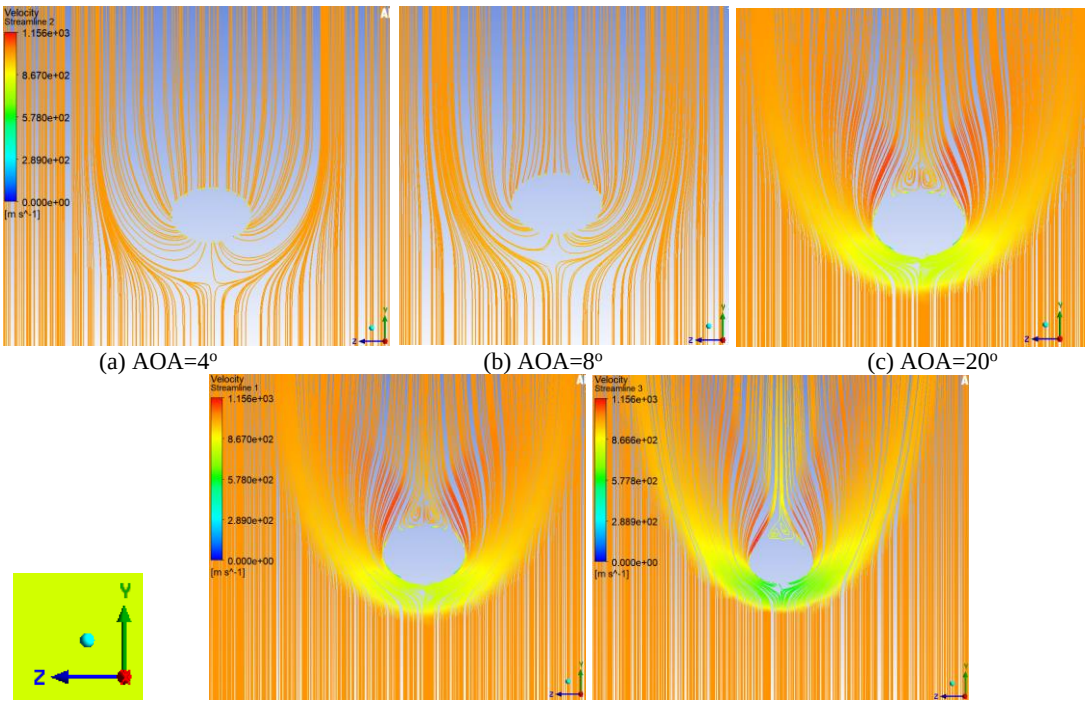

(a) AOA=4º (b) AOA=8º (c) AOA=20º

(d) AOA=30º (e) AOA=45º

Fig. 15 Velocity streamlines

As the angle of attack increases, the shock strength on the windward side increases, increasing the temperature downstream of the primary shock. This heat gets transferred to the leeward side, where the flow separation occurs, and hot vortex formation occurs at the center line, reducing the heating load on the leeward side.

4. CONCLUSION

Supersonic flow over elliptic cones with two different ellipticity ratios was simulated, and the aerodynamic coefficients were compared with that of the circular cone. Experimental results and theoretical relations available in the literature were used to validate the numerical results. The following conclusions were drawn from the study.

1) Cones with elliptical cross-sections produce higher lift when compared to cones with circular cross-sections, and the gain in lift increases with the ellipticity ratio. When the ellipticity ratio was increased from 1 to 3, the maximum increase in lift coefficient was 96% and 100% at Mach number 2.94 and 1.97, respectively

2) The increase in the lift coefficient for varying ellipticity ratio was because very high pressures were observed on the windward side, and this pressure reduced as the flow moved towards the leeward side.

3) Drag coefficient at zero lift remains constant with a change in ellipticity ratio. At zero angle of attack, all three considered cones produced the same drag.

4) At zero angle of attack, the shock formed around the elliptic cone appears circular in cross-section. The shock thickness was more along the minor axis plane when compared to that of the major axis plane.

5) As the angle of attack increased, the shock strength also increased on the windward side.

7) The computed flow regime at a higher angle of the attack showed a primary bow shock on the windward side and embedded shock on the leeward side, followed by flow separation and vortices.

CONFLICT OF INTEREST

The authors have no conflict of interest to disclose in this research work.

AUTHORS CONTRIBUTION

Vinod Kotebavi: Simulation, literature review, data collection, result analysis and writing the original draft. Rakesh S. G: Supervisor, review and editing.

REFERENCES

Allen., J. H., & E. W. Perkins (1951). *A study of effects of viscosity on flow over slender inclined bodies of revolution. NACA-TR-. 048.*

Bashkin, V. A., I. V. Egorov, & V. V. Pafnutiev (2008). Supersonic Viscous Perfect-Gas Flow Past a Slender Sharp Elliptic Cone. *Fluid Dynamics*, 43(6), 927–937. https://doi.org/10.1134/S0015462808060136

Bashkin, V. A., I. V. Egorov, D. V. Ivanov, & V. V. Pafnutiev (2009). Supersonic flow over sharp elliptical cones. *TsAGI Science Journal*, 40(6), 683–694. https://doi.org/10.1615/TsAGISciJ.v40.i6.50

Chen, J., F. Xiaoqiang, X. Bing, & W. Yi (2020). Shape optimization of the cross-section for noncircular

hypersonic missile forebody. *International Journal of Aerospace Engineering, Volume 2020, Article ID 8885494, 9 pages.* https://doi.org/10.1155/2020/8885494

Ishimatsu, T., & Morishita, E. (2005). Taylor-maccoll hypervelocity analytical solutions. *Transactions of the Japan Society for Aeronautical and Space Sciences 48* (159), 46-48. https://doi.org/10.2322/tjsass.48.46

Jorgensen, L. H. (1958). Elliptic cones alone and with wings at supersonic speeds. *NACA Rep. 1376*

Kaattari, G., E. (1970). *A method for predicting pressure on elliptic cones at supersonic speeds*. NASA Technical Note, NASA TN D-5952.

Kahane, A., & Solarski, A. (1953). Supersonic flow about slender bodies of elliptic cross section. *Journal of the Aeronautical Sciences*, 20(8). https://doi.org/10.2514/8.2719

Kopal, Z. (1947). *Tables of supersonic flow around cones (No. 1). Mass. Inst. of Technology.*

Krishnan, G., G. Akhil, & S. R. Nagaraja (2017). Drag reduction for hypersonic reentry vehicles. *International Journal of Mechanical Engineering and Technology*, 8(10), 878–885.

Nithin, D., & Vinod K. (2022). Performance characteristics of asymmetric body in hypersonic flow. *Advances in Mechanical and Materials Technology, Lecture Notes in Mechanical Engineering*, 1091-1099. https://doi.org/10.1007/978-981-16-2794-1_95

Pedro, P., Vassilis, T., & Daniel, R. (2013*). Accurate parabolic navier-stokes solutions of the supersonic flow around an elliptic cone.* 51st AIAA Aerospace Sciences Meeting including the New Horizons Forum and Aerospace Exposition. Grapevine, Texas. https://doi.org/10.2514/6.2013-670

Rahimi, A. B. (2012). Comparison of lift and drag forces for some conical bodies in supersonic flow using perturbation techniques. *Ije Transactions A*, 25(3): 231-238. https://doi.org/10.5829/idosi.ije.2012.25.03a.05

Rajesh, R., & Rakesh, S. G. (2017). Effect of dimensions of sharp spiked cylinder on the buzz phenomenon subjected to hypersonic flow. *International Journal of Fluid Mechanics Research*, 44(6):469–485. https://doi.org/10.1615/InterJFluidMechRes.2017019991

Rajesh, R., & Rakesh, S. G. (2020). Effect on the drag coefficient of various spiked cylinders during buzz phenomenon subjected to hypersonic flows. *Journal of the Brazilian Society of Mechanical Sciences and Engineering*, 42(6), 6. https://doi.org/10.1007/s40430-020-02384-5

Saiprakash, M., SenthilKumar, C., Sunil, G. K., Rampratap, S. P., Shanmugam, V., & Balu, G. (2019). Visualization of shock wave phenomenon around a sharp cone model at hypersonic mach number in a shock tunnel using high speed schlieren facility. *Journal of Applied Fluid Mechanics*, 12(2), 461-468. https://doi.org/10.29252/jafm.12.02.29250

Sanjay Krishna, M. S., & Kotebavi, V. (2021). *Study of aerodynamic and aerothermal characteristics of blunted power law bodies.* International Conference on Technology Innovation in Mechanical Engineering, TIME 2021, Lecture Notes in Mechanical Engineering. https://doi.org/10.1007/978-981-16-7909-4_66

Sims, J. L. (1964). *Tables for supersonic flow around right circular cones at zero angle of attack.* NASA-SP-3004

Sreekanth, N., Akhil, J., & Nagaraja, S. R. (2016). Design and analysis of secondary spike on blunt head. *Indian Journal of Science and Technology*, 9(45), 1-8. https://doi.org/10.17485/ijst/2016/v9i45/104649

Taylor, G. I., & Maccoll, J. W. (1933). The air pressure on a cone moving at high speeds—II. *Proceedings of the Royal Society of London. Series A*, Containing Papers of a Mathematical and Physical Character, 139(838), 298-311. https://doi.org/10.1098/rspa.1933.0017

Dyke, V. (1956). The slender elliptic cone as a model for non-linear supersonic flow theory. *Journal of Fluid Mechanics*, 1(1), 1–15. https://doi.org/10.1017/S0022112056000019

Wang, L. & Kong D. (2023). Study on pressure reconstruction method of explosion shock wave. *Journal of Applied Fluid Mechanics*,16(7), 1442-1454. https://doi.org/10.47176/jafm.16.07.1690